JOURNAL OF WATER AND LAND DEVELOPMENT
e-ISSN 2083-4535
Polish Academy of Sciences (PAN) Institute of Technology and Life Sciences – National Research Institute (ITP – PIB)

JOURNAL OF WATER AND LAND DEVELOPMENT
DOI: 10.24425/jwld.2026.157847
2026, No. 69 (IV–VI): 15–23

Hybrid cellular automata-artificial neural network land use change QGIS-MOLUSCE for urban watershed resilience

Rahmah Dara Lufira*[1)], Ussy Andawayanti[1)], Runi Asmaranto[1)], Ery Suhartanto[1)], Arrum Azzahra[1)], Rizki Tri Utami[1)], Irfan Tsany Rahmawan[2)]

[1)] Universitas Brawijaya, Faculty of Engineering, MT Haryono St, 167, 65145, Malang, Indonesia

[2)] Kumamoto University, Graduate School of Science and Technology, 860-8555, Kumamoto, Japan

* Corresponding author

RECEIVED 17.10.2025 ACCEPTED 07.01.2026 AVAILABLE ONLINE 30.04.2026

Abstract: Accurate land-use change (LUC) forecasts are essential for resilience-oriented planning in fast-urbanising watersheds. This study operationalises an open, reproducible cellular automata-artificial neural network (CA-ANN) workflow within the QGIS MOLUSCE plugin to simulate LUC in the Banjir Kanal Timur (BKT) watershed over 2004–2034. Multitemporal Landsat scenes (2004, 2014, 2024) were classified via maximum likelihood into five land-use classes, achieving overall accuracy (*OA*) of 90.7–94.9% and Kappa coefficients of 0.852–0.869; independent validation of the CA-ANN model against the 2024 map yielded Kappa = 0.829, indicating excellent agreement. Empirically, settlement expanded from 27.404 km^2 in 2004 to 43.158 km^2 in 2024 (>78% of the watershed), while forest declined from 22.467 to 5.775 km^2 and water bodies from 3.697 to 2.586 km^2. Forward simulation to 2034 indicates further settlement growth to 44.583 km^2 (80–81%), with forest contracting to 6.710 km^2 (12%) and water bodies to 2.776 km^2 (5%), signaling increasing imperviousness, reduced ecological buffering, and heightened flood and habitat-fragmentation risk. The hybrid CA-ANN model reproduces characteristic urban clustering and vegetation fragmentation and generates decision-oriented spatial layers, such as transition-potential surfaces and maps highlighting areas of rapid conversion and increased exposure. By embedding CA-ANN in an accessible QGIS-based pipeline, the study advances a transferable decision-support approach that links quantitative LUC forecasts and their uncertainties to enforceable growth boundaries, riparian buffers, and portfolios of low-impact development. Consequently, strengthens evidence-based zoning and urban watershed resilience planning.

Keywords: Banjir Kanal Timur Watershed, cellular automata-artificial neural network (CA-ANN), land use change, Modules for Land Use Change Evaluation (MOLUSCE), Quantum Geographic Information System (QGIS), urban watershed resilience

INTRODUCTION

Land-use change (LUC) is foundational to sustainable environmental management, urban planning, and natural conservation. Rapid population growth, infrastructure expansion, and climate variability are intensifying spatial and temporal transitions manifested as urban sprawl, deforestation, wetland loss, and degradation of ecologically sensitive zones (Dawid and Bielecka, 2022). Urban watersheds are especially affected by land conversion along transport corridors and peri-urban fringes, which cumulatively alters hydrologic pathways and degrades ecosystem functions. Advances in remote sensing and geospatial analysis particularly open source platforms such as Modules for Land Use Change Evaluation (MOLUSCE) enable the integration of satellite imagery, spatial drivers, and statistical learning for LUC analysis and prediction (Saputra *et al.*, 2024).

Despite these advances, generating reliable, decision-ready forecasts remains challenging in rapidly urbanising watersheds, where land-market signals, accessibility, and biophysical constraints interact across scales, creating nonlinear and heterogeneous patterns. Hybrid strategies that combine data-driven learning with spatial simulation therefore receive growing

attention. Cellular automata (CA) reproduce local clustering through neighbourhood effects but can underperform when non-spatial, multivariate drivers dominate (Ramadhan and Hidayati, 2022), whereas artificial neural networks (ANN) capture high-dimensional nonlinear relationships but lack explicit spatial context (Alipbeki *et al.*, 2024). Integrating CA to represent spatial autocorrelation with ANN to model multivariate driver effects offers a pathway (Tiye, 2025). However, many existing applications implement CA or ANN in stand-alone modelling environments or use MOLUSCE without fully exploiting hybrid CA-ANN capabilities and without systematically documenting driver selection, parameter calibration, and accuracy thresholds, which limits reproducibility and uptake by planning agencies (Yang *et al.*, 2017). The CA-ANN applications within MOLUSCE for highly urbanised, flood-control watersheds remain particularly limited, even though validated, high-resolution forecasts are needed for zoning, risk reduction, and ecological restoration (N'Danikou *et al.*, 2025). Within a GIS, integration underpins end-to-end pipelines from data preparation and training to scenario generation while analysis frameworks summarise to yield interpretable diagnostics for planners (Yang *et al.*, 2017).

This study develops an operational CA-ANN framework in QGIS MOLUSCE to predict land-use change in the Banjir Kanal Timur (BKT) watershed (2004–2034). The novelty lies in integrating high accuracy, multitemporal Landsat classifications with calibrated ANN transition potentials and CA spatial dynamics, accompanied by rigorous validation using confusion matrices and Kappa statistics. Methodologically, the distinctive contribution is a fully documented, end-to-end hybrid CA-ANN implementation inside an open-source GIS environment, where driver selection, parameter calibration, and accuracy thresholds are explicitly linked to decision needs in an urban watershed. Compared with previous CA- or ANN-based approaches, the proposed framework maintains explicit spatial dynamics while providing decision-ready layers that support enforceable growth boundaries, riparian setbacks, and portfolios of low-impact development. By capturing complex spatial and nonlinear interactions and transparently documenting inputs, parameters, and outputs, the workflow enhances reproducibility and transferability and offers practical guidance for translating LUC forecasts into evidence-based, resilience-oriented watershed governance.

MATERIALS AND METHOD

STUDY AREA

The Banjir Kanal Timur (BKT) watershed located in Semarang, Central Java, Indonesia (6°55'50"S–7°03'20"S; 110°25'00"E–110°29'10"E) covers 54.70 km^2 and extends 17.8 km as the main flood-control channel for eastern Semarang. Rapid residential and industrial growth has increased impervious surfaces, intensifying runoff and flood risk. Its transitional upland setting generates complex hydrology and elevates susceptibility to environmental degradation. The watershed boundary was delineated from River Basin Authority (RBA) Pemali Juana shapefiles in a Universal Transverse Mercator (UTM) framework (Fig. 1).

SATELLITE DATA ACQUISITION AND PREPROCESSING

Multitemporal satellite imagery for 2004 (Landsat-7 ETM+), 2014 (Landsat-8 OLI), and 2024 (Landsat-8 Surface Reflectance) was obtained from USGS Earth Explorer using scenes with cloud cover <10% and comparable seasonal windows to minimise phenological effects; datasets were georeferenced, clipped to the BKT boundary, and converted to 4-3-2 natural-colour composites with Band 8 pan-sharpening to enhance spatial detail with minimal spectral distortion (Zhang and Roy, 2016). All imagery was reprojected to WGS 1984 UTM Zone 49S, and preprocessing included atmospheric correction to surface reflectance, cloud/

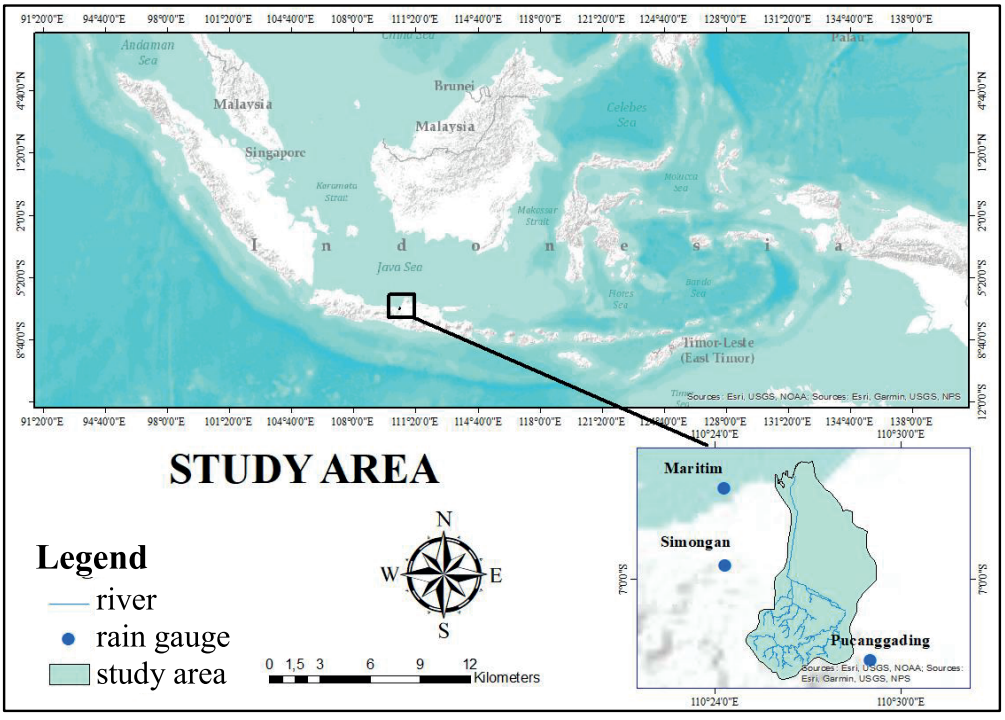

Fig. 1. Location of the Banjir Kanal Timur (BKT) watershed; source: own elaboration

shadow masking, and cross-date histogram matching to reduce radiometric disparities among sensors (Zhu, Wang and Woodcock, 2015). A conservative exterior buffer was retained and removed after classification to limit CA neighbourhood-edge artefacts, and all raster's were resampled to a 30 m grid aligned to the 2024 scene origin; the Landsat series was selected because it balances spatial resolution, spectral coverage, and temporal consistency (Roy *et al.*, 2014).

To ensure reproducibility, all three study years followed a consistent preprocessing chain in which candidate scenes were filtered in USGS Earth Explorer by path/row, intersection with the BKT watershed, and cloud cover (<10%) and downloaded with the associated quality-assessment (QA) band. Composite images (bands 1–7) were generated and visualised as 4-3-2 RGB for training-sample delineation, after which all scenes were projected to WGS 1984 UTM Zone 49S and clipped to the BKT watershed shapefile. Cloud and cloud-shadow pixels were masked using the QA-based cloud mask so that only cloud-free pixels entered classification and accuracy assessment. Finally, cross-date histogram matching was applied between corresponding bands before resampling all rasters to a common 30 m grid aligned to the 2024 reference scene, in line with good practice for multi-date Landsat-based land use and land cover (LULC) and runoff studies. The datasets, their providers, spatial characteristics, and roles in the modelling workflow are summarised in Table 1.

LAND USE CLASSIFICATION AND EXPLANATORY VARIABLES

Land-use was mapped using supervised maximum likelihood classification (MLC) in QGIS into five classes: built-up, vegetation, shrubland, water bodies, and open land. Training polygons were digitised from false-colour composites and cross-checked against Google Earth imagery, and under the MLC assumption of class-conditional normality pixels were assigned to the most likely class. Each date was classified with identical parameters, rasters were polygonised for area calculations, and procedures, class schema, and symbology were standardised across years to ensure comparability and seamless MOLUSCE ingestion (Kamaraj and Rangarajan, 2022). Three explanatory variables were used as predictors: distance to roads, distance to settlements, and slope derived from 30 m ASTER GDEM using the Horn algorithm and clipped to the watershed. All predictors were min.–max. normalised to the interval [0; 1], with *z*-scoring tested in sensitivity analyses; correlations and variance inflation factors (VIF) were examined to limit multicollinearity, and both distance variables were retained because they represent distinct policy-relevant gradients despite collinearity (Dormann *et al.*, 2013).

The choice of explanatory variables reflects data availability and main processes driving land use change in the BKT watershed. Distance to roads represents development pressure and corridor-driven growth along primary and toll networks, while distance to settlements captures infilling and edge expansion around built-up clusters. Slope serves as a proxy for construction feasibility and hydrological response, limiting conversion on steeper hillslopes that generate faster runoff. Other socio-economic drivers (e.g., land prices, detailed zoning, public transport accessibility) lack consistent coverage across all dates, so ad hoc or temporally inconsistent proxies were excluded to preserve a reproducible framework based on open spatial data.

ACCURACY ASSESSMENT

Classification accuracy was evaluated using proportionate stratified random sampling. Accuracy-assessment points were generated within QGIS and cross-verified against high-resolution Google Earth imagery. Confusion matrices for the 2004, 2014, and 2024 maps were used to compute overall accuracy (*OA*), user's accuracy (*UA*), producer's accuracy (*PA*), and the Kappa coefficient, following good-practice protocols for area estimation and accuracy assessment (Olofsson *et al.*, 2014). Sample size was calculated as:

$$n = \frac{N}{1 + N \cdot e^2} \tag{1}$$

$$OA = \frac{\sum_{i=1}^{K} n}{N} \; 100 \tag{2}$$

Table 1. Summary of main data sources and their use in the workflow

Dataset / layer	Year	Source	Type	Main use in this study
BKT watershed boundary and rivers	–	River Basin Authority (RBA) Pemali Juana	vector (shapefile)	watershed delineation and hydrologic context (study area, Fig. 1)
Landsat-7 ETM+	2004	USGS Earth Explorer	30 m multispectral	land-use classification and baseline map cellular automata-artificial neural network
Landsat-8 OLI	2014	USGS Earth Explorer	30 m multispectral	land-use classification and transition analysis
Landsat-8 Surface Reflectance	2024	USGS Earth Explorer	30 m surface reflectance	land-use classification, model validation, driver for 2034
ASTER GDEM	–	ASTER GDEM product	30 m raster	derivation of slope predictor (explanatory variable)
High-resolution Google Earth imagery	2004, 2014, 2024	Google Earth	sub-metric (visual)	support for training polygons and accuracy assessment

Explanations: BKT = Banjir Kanal Timur.
Source: own elaboration.

$$Kappa = \frac{N \sum_{i=1}^{K} n - \sum_{i=1}^{K} r_i \, c_i}{N^2 - \sum_{i=1}^{K} r_i \, c_i} \quad (3)$$

where: K = number of classes, n = number of correctly classified samples, r_i, c_i = row and column totals for class i in the confusion matrix, N = total of samples.

Using this expression with a 10% margin of error ($e = 0.1$), the minimum sample sizes for the accuracy assessment were 72, 75, and 78 points for the 2004, 2014, and 2024 land-use maps, respectively, which were then allocated proportionally to class area under the stratified design. The *OA* was computed as the proportion of correctly classified samples, while Kappa measured agreement beyond chance. All maps showed *OA* > 80% and Kappa > 0.80, confirming suitability for modelling. Validation compared simulated and observed 2024 maps, yielding strong Kappa agreement, and 2034 projections used the calibrated CA-ANN framework.

In addition to global metrics, class-specific *UA* and *PA* were inspected to diagnose residual confusion. The complement (1 − *OA*) was used as a map-wide empirical error margin. For temporal validation, CA-ANN calibrated in 2004–2014 simulated 2024 land use, with Kappa indicating strong agreement.

HYBRID CELLULAR AUTOMATA-ARTIFICIAL NEURAL NETWORK MODELLING FRAMEWORK

Land use change was simulated in QGIS using the MOLUSCE plugin, integrating an ANN to estimate transition potentials with a CA (Değermenci, 2023). A multi-layer perceptron (MLP) was trained on 2004–2014 transitions using distance to roads, settlements, and slope, tuned to minimise error and generate transition-potential surfaces (Zhou *et al.*, 2018). The CA module applied these surfaces within a 5×5 Moore neighbourhood using transition matrices (Hamad and Balzter, 2018). Calibration adjusted ANN and CA parameters and class-specific constraints, and the validated model projected 2034 land use from the 2014 and 2024 maps using the same drivers (Santé *et al.*, 2010).

The ANN calibration involved exploratory runs with varying numbers of hidden neurons and training iterations while monitoring mean-squared error, and the final configuration was selected once additional iterations or added complexity yielded only marginal reductions in training loss. The MOLUSCE stopping criterion thus combined a specified maximum iteration number with visual inspection of error-curve convergence. For the CA component, the number of iterations and class-specific transition constraints were similarly tuned so that simulated maps reproduced observed class totals and key spatial patterns for the calibration period within the accuracy margins reported in the accuracy assessment subsection. Taken together, this documented sequence, from standardised preprocessing and classification, through accuracy-aware calibration of ANN and CA components, to validated forward simulation-constitutes the core methodological advance: a transparent, end-to-end CA-ANN workflow in an open-source GIS aligned with urban-watershed decision needs.

RESULTS AND DISCUSSION

TEMPORAL DYNAMICS OF LAND USE (2004-2024)

The supervised classification of multi-temporal Landsat imagery revealed substantial spatiotemporal shifts in the BKT watershed over the past two decades. Forest cover declined from 22.467 km^2 in 2004 to 5.775 km^2 in 2024, a reduction exceeding 74% primarily due to conversion to residential land. Settlement areas expanded from 27.404 km^2 to 43.158 km^2, while water bodies contracted from 3.697 km^2 to 2.586 km^2, reflecting natural sedimentation and anthropogenic encroachment. These trajectories mirror urban-expansion patterns in rapidly developing tropical watersheds, where impervious surfaces replace forests and wetlands (Anhar *et al.*, 2024). The BKT watershed has experienced swift and significant land transformation, displaying patterns typical of unrestrained urbanisation (see Fig. 2). As of 2024, residential land comprised more than 78% of the total

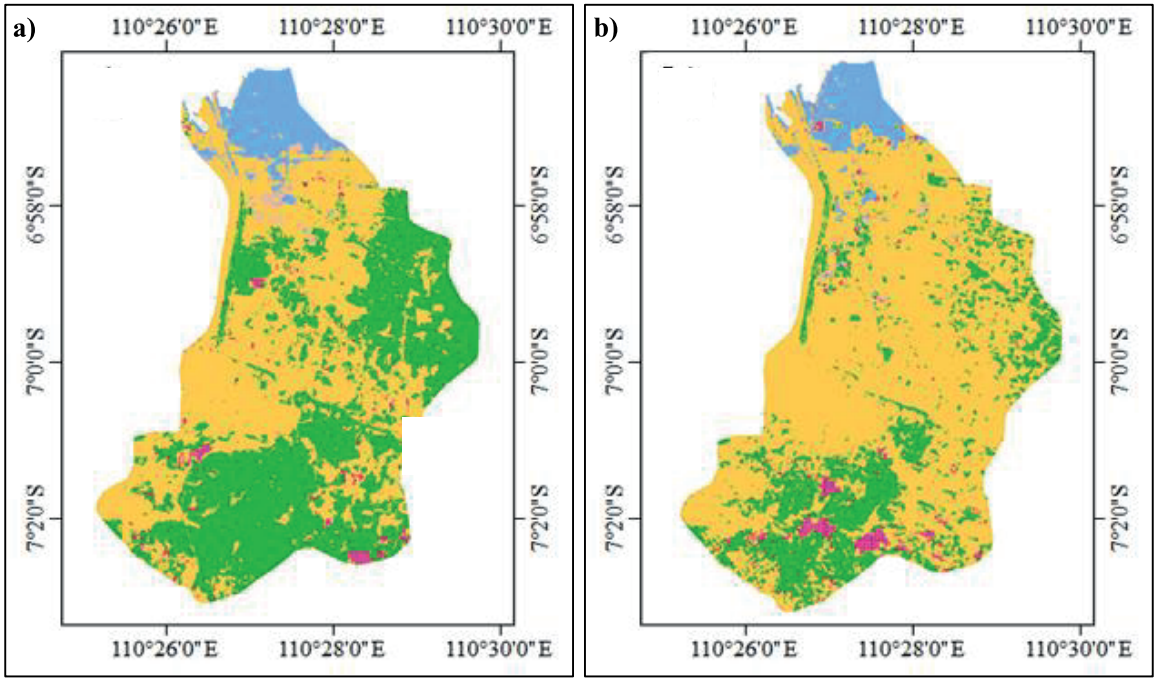

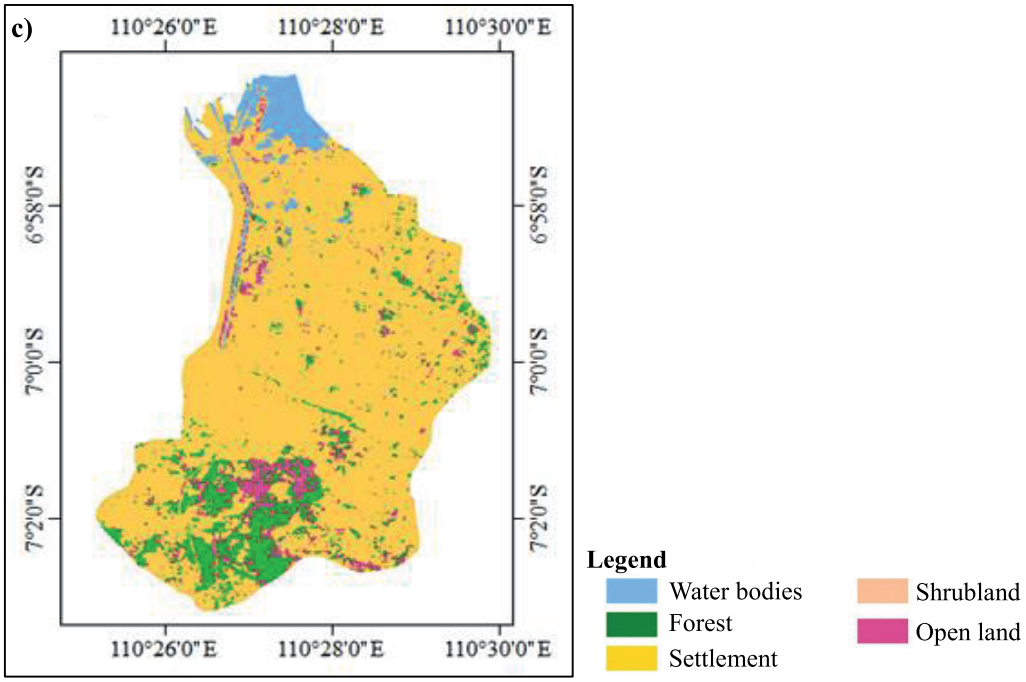

Fig. 2. Temporal dynamics of land use in the Banjir Kanal Timur (BKT) watershed: a) 2004, b) 2014, c) 2024; source: own study

watershed area, highlighting the prevalence of developed areas and the extent of land transformation.

Visual evidence in Figure 2 confirms extensive land transformation in the BKT watershed, typical of Southeast Asian urbanisation. The shift towards impervious cover suppresses infiltration, elevates stormwater runoff, and increases flood risk (Gholami *et al.*, 2023), consistent with findings that urban expansion displaces forests and wetlands in rapidly developing tropical watersheds (Vijay *et al.*, 2016). Vegetation loss and fragmentation weaken interception and evapotranspiration, while contraction of water bodies indicates reclamation and sediment infilling from upstream (Goldshleger *et al.*, 2014). Open land rose from 0.829 km^2 (2004) to 3.342 km^2 (2024), signalling sustained pressure on natural habitats. If current trajectories persist, by 2034 settlements and open land will expand, amplifying runoff, flood peaks, and extreme events (Nguyen *et al.*, 2021), while natural storage declines and legacy drainage proves inadequate (Ntajal *et al.*, 2020). Mitigation requires integrated green infrastructure, enforceable land-use controls, and restoration of riparian corridors (Kadir *et al.*, 2021). In interpreting these trends, the area estimates should be viewed the classification error margins reported in section "Classification accuracy and reliability"; while individual patch boundaries may be uncertain, the direction and magnitude of change at the watershed scale are robust. Quantitatively, these margins correspond to the empirical error rates (1 – *OA*) for each map year, which provide a simple bound on potential over- or underestimation of the reported class areas.

CLASSIFICATION ACCURACY AND RELIABILITY

Classification accuracy underpins the reliability of the land-use maps used in the CA-ANN simulations. Performance was evaluated using confusion matrices comparing classified labels with independent reference data to compute *OA*, *UA*, *PA*, and Kappa, capturing complementary aspects of agreement and highlighting recurrent misclassifications to refine training signatures. The minimum sample size for each date was derived using Slovin's formula with a 10% margin of error; for example, the 2024 dataset (N = 354 pixels) required at least 78 samples, while the 2014 and 2004 datasets required 75 and 72, respectively. Accuracy points were generated in ArcGIS (create accuracy assessment points), cross-checked against high-resolution Google Earth imagery, and their spatial distribution is shown in Figure 3.

The accuracy assessment results for 2004, 2014, and 2024 indicate *OA* values between 90.7 and 94.9%, with Kappa coefficients of 0.852–0.869, all exceeding thresholds of *OA* ≥ 90% and Kappa ≥ 0.85 and meeting the minimum accuracy standard of the Indonesian Geospatial Information Agency (Setyowati, 2021). Minor misclassifications occurred mainly between shrubland and residential areas, reflecting spectral similarity in transitional mosaics at medium resolution (Huang *et al.*, 2023). These errors are driven by mixed pixels along settlement edges, seasonal variation in vegetation condition, and limited training samples for narrow shrub belts, causing small semi-natural patches near housing clusters to be underestimated and compact settlement blocks to be slightly over-represented. In addition to these global metrics, class-specific *UA* and *PA* were examined to diagnose residual confusion, and the complement of overall accuracy (1 – *OA*) was used as a simple empirical error margin when interpreting model outputs. For the 2024 map, with *OA* = 0.91, the complementary value of 0.09 can be interpreted as an empirical error margin, implying that reported class areas should be viewed within ±9% of the stated values. This margin provides a lower bound on uncertainty propagated from classification into the CA-ANN projections, so projected class areas should be interpreted within this envelope rather than as exact values. Nevertheless, consistently high accuracies support the workflow's robustness, further gains are achievable through multi-source data fusion and multi-temporal Sentinel-2 time-series approaches, which have achieved *OA* >85% in rapidly changing landscapes (Debella-Gilo and Gjertsen, 2021).

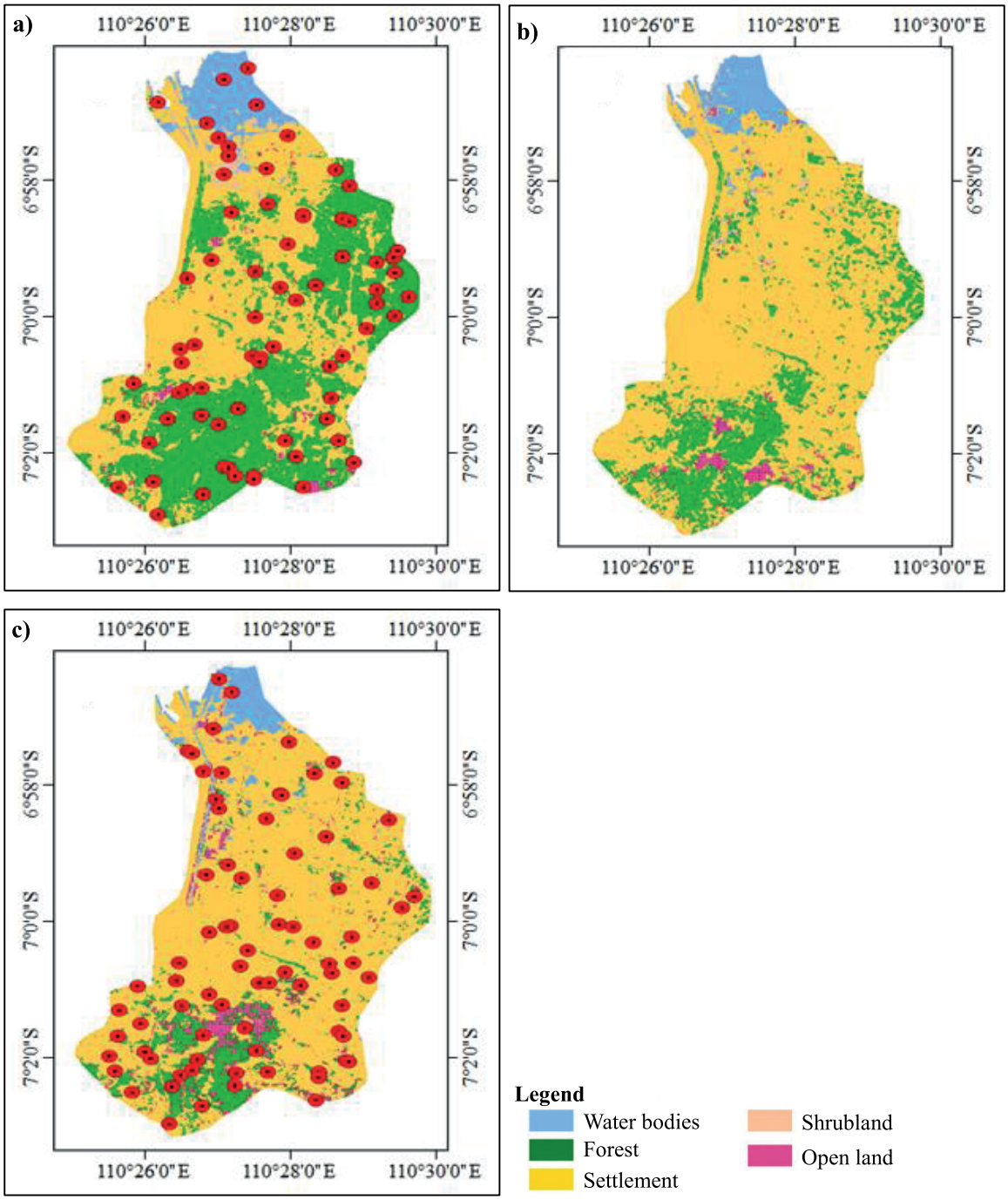

Fig. 3. Sample points used for accuracy assessment in the Banjir Kanal Timur (BKT) watershed: a) 2004, b) 2014, c) 2024; source: own study

PROJECTION TO 2034 USING CELLULAR AUTOMATA-ARTIFICIAL NEURAL NETWORK MODELLING

Using the MOLUSCE plugin in QGIS, we generated the 2034 projection with a hybrid framework that couples an ANN, which estimates transition potentials from distance to roads, distance to settlements, and slope, with a CA module that propagates neighbourhood effects. Model calibration used the 2004 and 2014 classified maps, while validation employed the 2024 map and yielded a Kappa of 0.829, indicating strong spatial agreement and supporting predictive reliability (Ali, Eddin and Ibrahim, 2009). Rapid early optimisation within 20–40 iterations are shown in Figure 4 and modest validation error fluctuation (0.075–0.095) – in Figure 5, consistent with stochastic mini-batch training rather than systematic overfitting.

The ANN tuning involved exploring alternative network settings and training iterations while monitoring mean-squared error; training was stopped once additional iterations produced only marginal improvements in validation error, providing an implicit stopping criterion based on error convergence rather than a fixed iteration count. The CA applied ANN-derived potentials on a 5×5 Moore neighbourhood, iteratively advancing to the target year using transition/probability matrices estimated from 2004–2014 changes. The cellular automata (CA) iterations

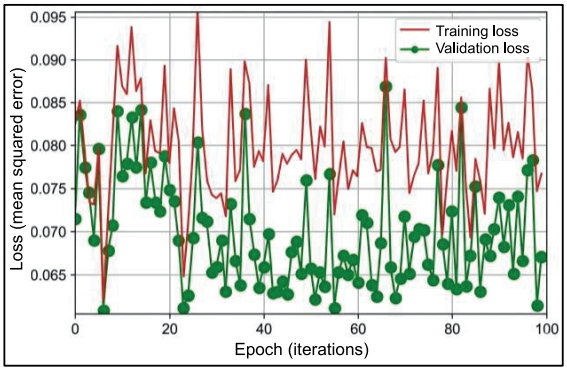

Fig. 4. Neural network learning curve for the artificial neural network component for the cellular automata-artificial neural network (CA-ANN) model; source: own study

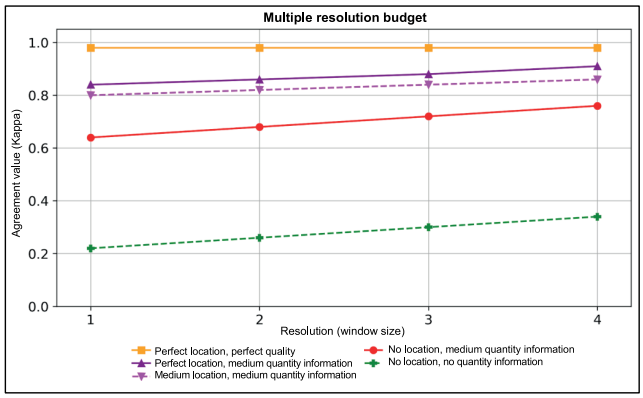

Fig. 5. Validation of the cellular automata-artificial neural network (CA-ANN) model against observed 2024 land use; source: own study

and class-specific transition constraints were adjusted so that the simulated 2024 map reproduced the observed class areas and main spatial patterns within the empirical error margins implied by the classification accuracy results. Because shrubland pixels near settlements are the primary source of confusion in the input maps, the model is less certain at fine-scale edges between built-up and semi-natural cover than for broader urban expansion fronts, so forecasts of total settlement extent and major growth corridors are reliable than cell-by-cell predictions of small residual vegetation patches within the urban matrix.

The validated model reproduced realistic urban clustering and vegetation fragmentation (Rahman *et al.*, 2023), and was then used to project 2034 land use from the 2014 and 2024 maps under identical drivers. This calibration–validation design corresponds to a temporal hold-out protocol, with 2004–2014 used for calibration and the independent 2024 map reserved solely for validation, rather than conventional *k*-fold cross-validation. The resulting Kappa of 0.829 lies at the upper end of the "very good" range typically reported for CA- or ANN-based land-use models, indicating that the added complexity of the hybrid CA-ANN approach yields predictive performance comparable to, or better than, many simpler CA or regression-based alternatives while retaining explicit spatial dynamics. The projections indicate that residential areas increase from 27.404 km^2 (49.63%) in 2004 to 44.583 km^2 (80.57%) in 2034, while forest cover declines from 22.467 km^2 (40.69%) to 6.710 km^2 (12.13%). Shrubland and open land decrease to 0.258 km^2 (0.47%) and 1.007 km^2 (1.82%), respectively, and water bodies decline from 3.697 km^2 (6.70%) to 2.776 km^2 (5.02%). Consistent with the classification analysis, these totals should be interpreted within the empirical uncertainty envelope defined by (1 − *OA*) for each map year (section "Classification accuracy and reliability"), rather than as exact point values. The land use changes for the BKT watershed are depicted in Figure 6.

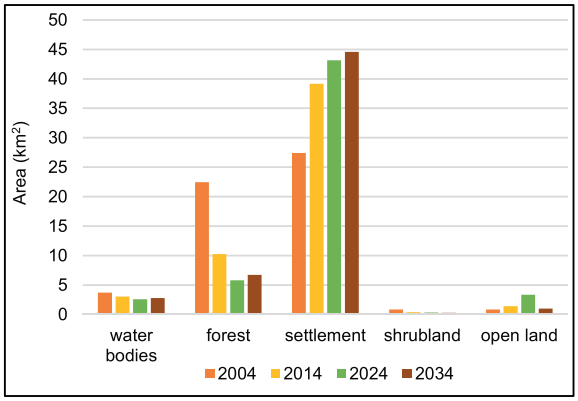

Fig. 6. Land use change in the Banjir Kanal Timur (BKT) watershed from 2004 to 2034; source: own study

From a hydrological perspective, increased impervious cover will reduce infiltration, elevate surface runoff, and raise flood peaks (Mahdi and Pagilla, 2021); while even modest shrubland decline remains critical for soil stabilisation, erosion control, and habitat provision (Cen, Peng and Dai, 2024). Spatially, the 2034 projection (Fig. 7) indicates intensified forest fragmentation smaller, isolated patches more vulnerable to edge effects, invasive species, and microclimatic shifts and reduced connectivity that constrains wildlife movement and biodiversity resilience (Garvey *et al.*, 2022).

Mitigation strategies must include the restoration of riparian buffers, integration of low impact development (LID) practices such as permeable pavements, bioswales, and green roofs (Wang *et al.*, 2017). With settlement 80.6% and forest 12.1%

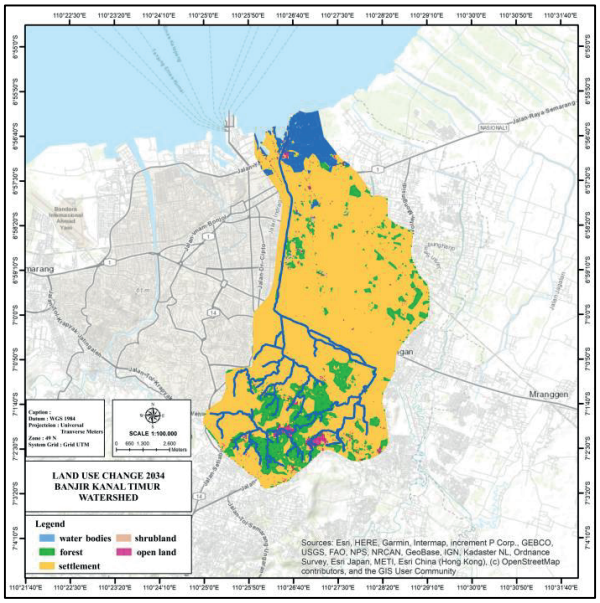

Fig. 7. Predicted land use distribution in the Banjir Kanal Timur (BKT) watershed by 2034; source: own study

by 2034, higher runoff and flood peaks alongside habitat fragmentation are anticipated (Harianto *et al.*, 2022). Similar hybrid CA-ANN applications in rapidly urbanising watersheds in developing regions report a strong dominance of built-up expansion at the expense of natural covers, with corridor-driven growth and peri-urban forest loss as characteristic trajectories under weak land-use control (N'Danikou *et al.*, 2025). Compared with these studies, the present framework places greater emphasis on an explicitly documented, accuracy-aware implementation within QGIS MOLUSCE plugin that is directly aligned with urban watershed resilience planning. Compared with these studies, the present framework places greater emphasis on an explicitly documented, accuracy-aware implementation within MOLUSCE that is directly aligned with urban watershed resilience planning. In this context, the CA-ANN outputs should be regarded as spatially explicit, probabilistic scenarios constrained by the classification and validation errors discussed above: although local cell-by-cell allocations inevitably contain uncertainty, broader spatial patterns, such as expansion along arterial corridors and contraction of core forest, constitute robust signals for comparative model evaluation and risk-based planning. The resulting decision-support products identify growth-boundary breaches, arterial-road corridors requiring tighter zoning and density control, priority reaches for riparian restoration and LID retrofits, and connectivity gaps where pocket parks and street-tree networks can buffer edge effects and enhance urban biodiversity (Zhou *et al.*, 2019). Agencies can use these baselines to evaluate plan compliance and sustainability outcomes annually.

CONCLUSIONS

This study operationalised a transparent, open-source cellular automata-artificial neural network (CA-ANN) workflow within QGIS MOLUSCE plugin to forecast land-use changes in the Banjir Kanal Timur (BKT) watershed, integrating multitemporal Landsat classifications (2004, 2014, 2024) with ANN-derived transition potentials and CA neighbourhood dynamics. Classification performance was high (*OA* = 90.7–94.9%, Kappa = 0.852–0.869), and validation against the 2024 map yielded Kappa = 0.829. Empirically, forest declined from 22.467 to 5.775 km^2 while settlement increased from 27.404 to 43.158 km^2 (>78% of the watershed by 2024); projections to 2034 indicate settlements of 44.583 km^2 (80.6%), forest 6.710 km^2 (12.1%), and water 2.776 km^2 (5.0%), implying increased imperviousness and hydrological pressure.

For urban planners and river-basin agencies, the decision-ready products support enforceable growth boundaries, zoning, and prioritisation of riparian-buffer restoration and low impact development (LID) to moderate runoff and maintain ecological functions. The workflow is most applicable to medium-sized, rapidly urbanising watersheds with comparable data and institutional capacity; data-poor or contrasting socio-ecological settings require recalibration and local testing. Key limitations include a restricted driver set, 30 m resolution, and residual confusion among transitional classes. Future work should quantify uncertainty, apply cross-validation, enrich predictors and neighbourhood rules, and couple land-use projections with hydrologic and hydraulic models to assess flood risk and resilience.

ACKNOWLEDGEMENT

We thank data providers such as the Water Resources Public Works Agency (WRPWA) of Central Java and the River Basin Authority (RBA) Pemali Juana. We truly appreciate and thank the collaborative efforts of all partners, researchers, stakeholders to understand hydrology, and design management plans with due regard to environmental and ecological perspectives.

AUTHOR CONTRIBUTIONS

1st Author (23%): study design, data collection, manuscript preparation, and literature search. 2nd Author (12%): statistical analysis and data interpretation. 3rd Author (12%): statistical analysis and data interpretation. 4th Author (15%): statistical analysis, data interpretation, manuscript preparation. 5th Author (15%): data collection and statistical analysis. 6th Author (12%): data collection and statistical analysis. 7th Author (11%): data collection and literature search.

CONFLICT OF INTEREST

All authors declare no conflict of interest.

REFERENCES

Ali, A.E., Eddin, E. and Ibrahim, A. (2009) "Mapping waste-disposal sites in Riyadh using RADARSAT imagery," *Journal of King Saud University – Engineering Sciences*, 21(1), pp. 7–13. Available at: https://doi.org/10.1016/S1018-3639(18)30518-X.

Alipbeki, O. *et al.* (2024) "Analysis and prediction of land use/land cover changes in Korgalzhyn District, Kazakhstan," *Agronomy*, 14(2), 268. Available at: https://doi.org/10.3390/agronomy14020268.

Anhar, A. *et al.* (2024) "Changes in land use and land cover in forest areas in Bener Meriah and Aceh Tengah Districts, Indonesia," *IOP Conference Series: Earth and Environmental Science*, 1297, 012085. Available at: https://doi.org/10.1088/1755-1315/1297/1/012085.

Cen, L., Peng, X. and Dai, Q. (2024) "Response of the stability of soil aggregates and erodibility to land use patterns in wetland ecosystems of Karst Plateau," *Forests*, 15(4), 599. Available at: https://doi.org/10.3390/f15040599.

Dawid, W. and Bielecka, E. (2022) "GIS-based land cover analysis and prediction based on open-source software and data," *Quaestiones Geographicae*, 41(4), pp. 91–106. Available at: https://doi.org/10.2478/quageo-2022-0026.

Debella-Gilo, M. and Gjertsen, A.K. (2021) "Mapping seasonal agricultural land use types using deep learning on Sentinel-2 image time series," *Remote Sensing*, 13(2), 289. Available at: https://doi.org/10.3390/rs13020289.

Değermenci, A.S. (2023) "Spatio-temporal change analysis and prediction of land use and land cover changes using CA-ANN model," *Environmental Monitoring and Assessment*, 195(10), 11848. Available at: https://doi.org/10.1007/s10661-023-11848-9.

Dormann, C.F. *et al.* (2013) "Collinearity: A review of methods to deal with it and a simulation study evaluating their performance," *Ecography*, 36(1), pp. 27–46. Available at: https://doi.org/10.1111/j.1600-0587.2012.07348.x.

Garvey, S.M. *et al.* (2022) "Diverging patterns at the forest edge: soil respiration dynamics of fragmented forests in urban and rural areas," *Global Change Biology*, 28(9), pp. 3094–3109. Available at: https://doi.org/10.1111/gcb.16099.

Gholami, F. *et al.* (2023) "Spatial-temporal analysis of various land use classifications and their long-term alteration's impact on hydrological components: using remote sensing, SAGA-GIS, and ArcSWAT model," *Environmental Science: Water Research & Technology*, 9(4), pp. 1161–1181. Available at: https://doi.org/10.1039/D2EW00138A.

Goldshleger, N. *et al.* (2014) "Influence of land use on the quality of runoff along Israel's coastal strip (demonstrated in the cities of Herzliya and Ra'anana)," *Hydrological Processes*, 28(4), pp. 2144–2157. Available at: https://doi.org/10.1002/hyp.10220.

Hamad, R. and Balzter, H. (2018) "Predicting land use/land cover changes using a CA-Markov model under two different scenarios," *Sustainability*, 10(10), 3421. Available at: https://doi.org/10.3390/su10103421.

Harianto, E. *et al.* (2022) "Water and land efficiency in eel (*Anguilla bicolor bicolor*) rearing in development of urban aquaculture through vertical aquaculture system," *IOP Conference Series: Earth and Environmental Science*, 1033, 012013. Available at: https://doi.org/10.1088/1755-1315/1033/1/012013.

Huang, Y. *et al.* (2023) "Tree species classification in UAV remote sensing images based on super-resolution reconstruction and deep learning," *Remote Sensing*, 15(11), 2942. Available at: https://doi.org/10.3390/rs15112942.

Kadir, A. *et al.* (2021) "Integrated approach to quantify the impact of land use and land cover changes on water quality of Surma River, Sylhet, Bangladesh," *Water*, 14(1), 17. Available at: https://doi.org/10.3390/w14010017.

Kamaraj, M. and Rangarajan, S. (2022) "Predicting the future land use and land cover changes for Bhavani basin, Tamil Nadu, India, using QGIS MOLUSCE plugin," *Environmental Science and Pollution Research*, 29(63), pp. 86337–86348. Available at: https://doi.org/10.1007/s11356-021-17904-6.

Mahdi, N. and Pagilla, K. (2021) "Continuous simulation of highly urbanized watershed to quantify nutrients' loadings," *Water*, 13(20), 2910. Available at: https://doi.org/10.3390/w13202910.

N'Danikou, K.A. *et al.* (2025) "Change monitoring and assessment of land use and land cover for the municipality of Ouessè in Benin by the Modules for Land Use Change Evaluation plugin," *International Journal of Agricultural and Environmental Information Systems*, 16(1), pp. 1–18. Available at: https://doi.org/10.4018/IJAEIS.369814.

Nguyen, H.D. *et al.* (2021) "Predicting future urban flood risk using land change and hydraulic modeling in a river watershed in the central province of Vietnam," *Remote Sensing*, 13(2), 262. Available at: https://doi.org/10.3390/rs13020262.

Ntajal, J. *et al.* (2020) "Influences of land-use dynamics and surface water systems interactions on water-related infectious diseases A systematic review," *Water*, 12(3), 631. Available at: https://doi.org/10.3390/w12030631.

Olofsson, P. *et al.* (2014) "Good practices for estimating area and assessing accuracy of land change," *Remote Sensing of Environment*, 148, pp. 42–57. Available at: https://doi.org/10.1016/j.rse.2014.02.015.

Rahman, M. *et al.* (2023) "Assessing the influence of land cover and climate change impacts on runoff patterns using CA-ANN model and CMIP6 data," *ISPRS International Journal of Geo-Information*, 12(10), 401. Available at: https://doi.org/10.3390/ijgi12100401.

Ramadhan, G.F. and Hidayati, I.N. (2022) "Prediction and simulation of land use and land cover changes using open source QGIS: A case study of Purwokerto, Central Java, Indonesia," *Indonesian Journal of Geography*, 54(3), pp. 344–351. Available at: https://doi.org/10.22146/ijg.68702.

Roy, D.P. *et al.* (2014) 'Landsat-8: Science and product vision for terrestrial global change research," *Remote Sensing of Environment*, 145, pp. 154–172. Available at: https://doi.org/10.1016/j.rse.2014.02.001.

Santé, I. *et al.* (2010) "Cellular automata models for the simulation of real-world urban processes: a review and analysis," *Landscape and Urban Planning*, 96(2), pp. 108–122. Available at: https://doi.org/10.1016/j.landurbplan.2010.03.001.

Saputra, A.N. *et al.* (2024) "Modeling of land cover changes in Banjarbaru City South Kalimantan Province," *Jurnal Geografi*, 16(1), pp. 89–100. Available at: https://doi.org/10.24114/jg.v16i1.48121.

Setyowati, D.L. (2021) "Assessment of watershed carrying capacity and land use change on flood vulnerability areas in Semarang City," *Forum Geografi in Indonesia*, 35(2), Available at: https://doi.org/10.23917/forgeo.v35i2.15542.

Tiye, F.S. (2025) "Modeling land use and land cover dynamics of Bale Mountains National Park using Google Earth Engine and cellular automata-artificial neural network (CA-ANN) model," *PLOS One*, 20(1), 0320428. Available at: https://doi.org/10.1371/journal.pone.0320428.

Vijay, V. *et al.* (2016) "The impacts of oil palm on recent deforestation and biodiversity loss," *PLOS One*, 11(7), 0159668. Available at: https://doi.org/10.1371/journal.pone.0159668.

Wang, M. *et al.* (2017) "Future scenarios modelling of urban stormwater management response to impacts of climate change and urbanization," *Clean – Soil, Air, Water*, 45(8), 1700111. Available at: https://doi.org/10.1002/clen.201700111.

Yang, Y. *et al.* (2017) "Use of intensity analysis to measure land use changes from 1932 to 2005 in Zhenlai County, Northeast China," *Chinese Geographical Science*, 27(3), pp. 441–455. Available at: https://doi.org/10.1007/s11769-017-0876-8.

Zhang, H.K. and Roy, D.P. (2016) "Computationally inexpensive Landsat-8 operational land imager (OLI) surface reflectance," *Remote Sensing*, 8(3), 180. Available at: https://doi.org/10.3390/rs8030180.

Zhou, L. *et al.* (2018) "An approach to evaluate comprehensive plan and identify priority lands for future land use development to conserve more ecological values," *Sustainability*, 10(1), 126. Available at: https://doi.org/10.3390/su10010126.

Zhou, Z. *et al.* (2019) "Storm catalog-based analysis of rainfall heterogeneity and frequency in a complex terrain," *Water Resources Research*, 55(3), pp. 1871–1889. Available at: https://doi.org/10.1029/2018WR023567.

Zhu, Z., Wang, S. and Woodcock, C.E. (2015) "Improvement and expansion of the Fmask algorithm: Cloud, cloud shadow, and snow detection for Landsats 4–7, 8, and Sentinel-2 images," *Remote Sensing of Environment*, 159, pp. 269–277. Available at: https://doi.org/10.1016/j.rse.2014.12.014.